

## Structural and Functional Analysis of the NLRP4 Pyrin Domain

Clarissa Eibl,<sup>†</sup> Simina Grigoriu,<sup>‡</sup> Manuel Hessenberger,<sup>†</sup> Julia Wenger,<sup>†</sup> Sandra Puehringer,<sup>§,||</sup> Anderson S. Pinheiro,<sup>‡</sup> Roland N. Wagner,<sup>†</sup> Martina Proell,<sup>†</sup> John C. Reed,<sup>†</sup> Rebecca Page,<sup>#</sup> Kay Diederichs,<sup>\*,@</sup> and Wolfgang Peti<sup>\*,‡,V</sup>

<sup>†</sup>Department of Molecular Biology, University of Salzburg, 5020 Salzburg, Austria

<sup>‡</sup>Department of Molecular Pharmacology, Physiology and Biotechnology, Brown University, Providence, Rhode Island 02903, United States

<sup>§</sup>Institute for Soft Matter and Functional Materials, Macromolecular Crystallography, Helmholtz-Zentrum Berlin für Materialien und Energie, 12489 Berlin, Germany

<sup>||</sup>Department of Biology and Chemistry, Freie Universität Berlin, 14195 Berlin, Germany

<sup>†</sup>Sanford-Burnham Medical Research Institute, La Jolla, California 92037, United States

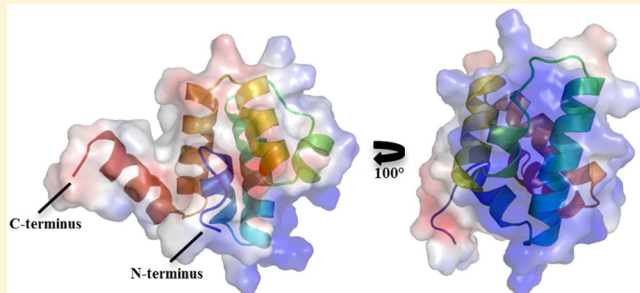
<sup>#</sup>Department of Molecular Biology, Cell Biology and Biochemistry, Brown University, Providence, Rhode Island 02903, United States

<sup>@</sup>Department of Biology, University of Konstanz, 78457 Konstanz, Germany

<sup>V</sup>Department of Chemistry, Brown University, Providence, Rhode Island 02912, United States

### Supporting Information

**ABSTRACT:** NLRP4 is a member of the nucleotide-binding and leucine-rich repeat receptor (NLR) family of cytosolic receptors and a member of an inflammation signaling cascade. Here, we present the crystal structure of the NLRP4 pyrin domain (PYD) at 2.3 Å resolution. The NLRP4 PYD is a member of the death domain (DD) superfamily and adopts a DD fold consisting of six  $\alpha$ -helices tightly packed around a hydrophobic core, with a highly charged surface that is typical of PYDs. Importantly, however, we identified several differences between the NLRP4 PYD crystal structure and other PYD structures that are significant enough to affect NLRP4 function and its interactions with binding partners. Notably, the length of helix  $\alpha$ 3 and the  $\alpha$ 2– $\alpha$ 3 connecting loop in the NLRP4 PYD are unique among PYDs. The apoptosis-associated speck-like protein containing a CARD (ASC) is an adaptor protein whose interactions with a number of distinct PYDs are believed to be critical for activation of the inflammatory response. Here, we use co-immunoprecipitation, yeast two-hybrid, and nuclear magnetic resonance chemical shift perturbation analysis to demonstrate that, despite being important for activation of the inflammatory response and sharing several similarities with other known ASC-interacting PYDs (i.e., ASC2), NLRP4 does not interact with the adaptor protein ASC. Thus, we propose that the factors governing homotypic PYD interactions are more complex than the currently accepted model, which states that complementary charged surfaces are the main determinants of PYD–PYD interaction specificity.



Multicellular organisms have evolved two distinct types of immune responses against foreign invaders: the faster innate immune system and the delayed adaptive immune system. Innate immunity forms the first line of defense against invading pathogens and harmful environmental factors by detecting danger- and pathogen-associated molecular patterns (DAMPs and PAMPs, respectively) via diverse pattern recognition receptors (PRRs). Whereas the membrane-anchored Toll-like receptors represent the classical PRRs, the cytosolic nucleotide-binding and leucine-rich repeat-containing receptors (NLRs, alternatively named NBD-LRR or CATER-PILLER) are essential for the recognition of cytosolic PAMPs not intercepted by membrane-bound receptors (for reviews, see refs 1–3).

NLR genes encode large multidomain proteins with a conserved tripartite domain architecture characterized by (1) C-terminal leucine-rich repeats (LRRs) necessary for ligand binding, (2) a central nucleotide-binding and oligomerization domain termed the NACHT domain, and (3) an N-terminal effector domain most commonly in the form of either a pyrin domain (PYD), a caspase activation and recruitment domain (CARD), or a baculovirus inhibitor repeat domain (BIR). These effector domains bind downstream signaling molecules, ultimately leading to activation of various protein kinases,

**Received:** May 29, 2012

**Revised:** August 28, 2012

**Published:** August 28, 2012

transcription factors, proteases, and other components of host defense and inflammatory responses.<sup>4–6</sup>

NLRs are divided into three subfamilies according to the identity of their N-terminal effector domains. NLRs containing a PYD (NLRPs) form the largest subfamily, with 14 members in total (NLRP1–NLRP14) in humans.<sup>6</sup> NLRP1 and NLRP3, the best-characterized NLRPs, activate the inflammatory immune response by detecting cytosolic PAMPs via their C-terminal LRR domains. Once active, NLRP1 and NLRP3 oligomerize via their central NACHT domains. Finally, the N-terminal PYDs recruit the adaptor protein ASC via homotypic PYD–PYD interactions, resulting in recruitment of pro-caspase 1 molecules via homotypic CARD–CARD interactions.<sup>4</sup> The ensuing multicomponent signaling platform, termed the inflammasome, is analogous to the well-studied Apaf-1 apoptosome.<sup>7</sup> Formation of the inflammasome results in the autoproteolytic activation of caspase 1, which, in turn, cleaves proinflammatory cytokines such as pro-IL-1 $\beta$  and pro-IL-18 into their mature forms.<sup>4,5,8</sup> Polymorphisms in NLRP1 and NLRP3 are associated with susceptibility to chronic inflammatory disorders, such as Crohn's disease, Muckle Wells syndrome, and familial cold autoimmune syndrome, highlighting the importance of these receptors in innate immunity.<sup>9,10</sup> A detailed understanding of the molecular mechanisms underlying NLR signaling is of great biological and medical importance, being critical for the more efficient treatment of these diseases.

Recent reports have identified novel, significantly divergent functions for NLRPs, in addition to their already well-established proinflammatory functions.<sup>11</sup> This is especially true for NLRP4 (113 kDa; also known as PAN2, Nalp4, or PYPAF4), which is strongly expressed in several diverse tissues, including placenta, testis, oocytes, spleen, pancreas, lung, liver, kidney, and thymus.<sup>12–14</sup> NLRP4 has recently been reported as a negative regulator of autophagy and type I interferon signaling, resulting from the interaction of its NACHT domain with Beclin1 and TBK1, respectively.<sup>12,15</sup> Furthermore, NLRP4 was identified as an inhibitor of TNF- $\alpha$ - and IL-1 $\beta$ -mediated NF- $\kappa$ B activation, which is achieved through an interaction with IKK $\alpha$ . The PYD of NLRP4 is necessary for this inhibitory effect on NF- $\kappa$ B, underscoring its importance as a critical regulator of inflammation signaling pathways.<sup>12,13,15</sup>

Several PYD structures have been determined recently. These structures showed a high degree of conservation of their three-dimensional organization and surface charge distribution. Thus, the molecular basis for the specificity of their differential interactions remains poorly understood.<sup>16–20</sup> Here, we report the crystal structure of human NLRP4 PYD at 2.3 Å resolution, alongside interaction studies with the adaptor protein ASC, and provide novel insights into the complexity of PYD interactions and the factors dictating their specificity.

## ■ EXPERIMENTAL PROCEDURES

**Protein Expression and Purification.** The coding region of NLRP4 PYD (residues Met1–Leu110) was amplified via polymerase chain reaction (PCR) using human NLRP4 cDNA (GenBank entry BC050326) as a DNA template and cloned into the pET28a stop plasmid (Invitrogen), with an N-terminal His<sub>6</sub> tag followed by a thrombin cleavage site. *Escherichia coli* BL21 Star(DE3) (Invitrogen) cells were transformed with the sequence-verified NLRP4 PYD plasmid (Eurofins MWG Operon, Ebersberg, Germany) and grown in 600 mL of LB medium to an OD<sub>600</sub> of 0.8, at which point protein expression

was induced with 420 μM IPTG at 25 °C for 5 h. Harvested cells were resuspended in lysis buffer I [50 mM KH<sub>2</sub>PO<sub>4</sub> (pH 7.8), 300 mM NaCl, 5 mM imidazole, and 0.1 mg/mL lysozyme] and stored at –20 °C until they were lysed by sonication. The lysate containing His<sub>6</sub>-tagged NLRP4 PYD was clarified by centrifugation and loaded on 800 μL of pre-equilibrated Ni<sup>2+</sup>-NTA resin (Qiagen) for immobilized metal affinity chromatography. The beads were washed with 15 mL of wash buffer I [20 mM Tris (pH 8.0), 1 M NaCl, and 20 mM imidazole], followed by 15 mL of wash buffer II [20 mM Tris (pH 8.0), 1 M NaCl, and 40 mM imidazole]. NLRP4 was eluted by thrombin digestion (Sigma Aldrich). The untagged NLRP4 PYD was further purified using a Superdex 75 10/300 size exclusion column (SEC) (GE Healthcare) equilibrated in size exclusion buffer I [20 mM Tris (pH 8.0), 150 mM NaCl, and 5 mM TCEP]. The SEC column was calibrated using the Gel Filtration Calibration Kit (GE Healthcare) according to the manufacturer's protocol to detect the oligomerization state of the NLRP4 PYD. Fractions containing the NLRP4 PYD were combined and concentrated by evaporation to 1.5 mg/mL. Selenomethionine (SeMet)-labeled protein was expressed in minimal medium (Molecular Dimensions) and purified under identical conditions. The <sup>15</sup>N-labeled NLRP4 PYD was expressed in M9 minimal medium containing 4 g/L [<sup>12</sup>C]-D-glucose and 1 g/L <sup>15</sup>NH<sub>4</sub>Cl (Cambridge Isotope Laboratories, Cambridge, MA) as the sole carbon and nitrogen sources, respectively, and purified under identical conditions. Prior to NMR experiments, the <sup>15</sup>N-labeled NLRP4 PYD was exchanged into NMR buffer [20 mM sodium phosphate (pH 7.2), 100 mM NaCl, and 0.5 mM TCEP].

The L25A solubility-enhancing mutation in the ASC PYD was introduced via overlap extension mutagenesis, and the His<sub>6</sub>-tagged L25A ASC PYD (residues 1–94) was expressed and purified as previously described for the wild-type ASC PYD.<sup>20</sup> To attach a GB1 solubility tag, the L25A ASC PYD (hereafter termed ASC PYD) sequence was amplified via PCR and subcloned into the pETRP1B-GB1 bacterial expression vector (in-house), which encodes an N-terminal His<sub>6</sub> tag followed by a TEV (tobacco etch virus) protease cleavage site and a noncleavable GB1 solubility tag that is separated from the ASC PYD by a four-amino acid linker (AAEF). For large-scale expression of the GB1-ASC L25A PYD (hereafter termed GB1-ASC PYD), the sequence-verified (Beckman Genomics) GB1-ASC PYD construct was transformed into BL21-CodonPlus (DE3)-RIL cells (Agilent), and 1 L cultures were grown in LB medium to an OD<sub>600</sub> of 0.7. Cultures were chilled at 4 °C for 1 h, and protein expression was induced with 1 mM IPTG for 18 h with vigorous shaking (250 rpm) at 18 °C. Cell pellets were harvested (6000g for 15 min at 4 °C), and cell paste was stored at –80 °C. The <sup>15</sup>N-labeled ASC PYD and GB1-ASC PYD were expressed as described for the <sup>15</sup>N-labeled NLRP4 PYD. The GB1-ASC PYD (<sup>15</sup>N-labeled and unlabeled) was purified as follows. The cell pellet was thawed and resuspended in lysis buffer II [50 mM Tris (pH 8.0), 500 mM NaCl, 5 mM imidazole, 0.1% Triton X-100, and EDTA-free protease inhibitor tablets (Roche)] and lysed using high-pressure cell homogenization (Avestin C3 Emulsiflex). The clarified cell lysate (35000g for 50 min at 4 °C) was loaded onto a HisTrap HP column (GE Healthcare) equilibrated with His-tag buffer A [50 mM Tris (pH 8.0), 500 mM NaCl, and 5 mM imidazole], and the protein was eluted with a 5 to 500 mM imidazole gradient over 60 min. Fractions containing the His<sub>6</sub>-tagged GB1-ASC PYD, as determined by sodium dodecyl sulfate–

Table 1. Summary of Crystal Parameters, Data Collection, and Refinement Statistics

	Data Collection			
space group unit cell parameters	$\lambda 1$ MADSe <sup>a</sup>	$\lambda 2$ MADSe <sup>a</sup>	$\lambda 3$ MADSe <sup>a</sup>	$\lambda 4$ native <sup>a</sup>
wavelength (Å)	0.97958	0.97973	0.9719	0.9184
resolution (Å)	32.82–2.82	32.86–2.76	32.89–2.88	40.76–2.28
highest-resolution shell (Å)	2.89–2.82	2.83–2.76	2.96–2.88	2.42–2.28
mosaicity (deg)	0.241	0.235	0.241	0.136
no. of reflections <sup>b</sup>	67335 (3276)	76639 (5174)	69396 (5428)	102943 (16562)
no. of unique reflections <sup>b</sup>	12689 (938) <sup>c</sup>	13680 (1076) <sup>c</sup>	12091 (930) <sup>c</sup>	13300 (2097)
completeness <sup>b</sup> (%)	99.4 (99.6)	99.7 (100)	99.7 (100)	99.9 (99.9)
multiplicity <sup>b</sup>	5.3 (3.5)	5.6 (4.8)	5.7 (5.8)	7.7 (7.9)
mean $I/\sigma(I)^b$	18.0 (2.1)	18.6 (1.8)	20.2 (2.2)	20.8 (3.0)
$R_{\text{meas}}^{b,d}$ (%)	6.5 (65.6)	6.5 (91.4)	6.4 (77.3)	6.3 (87.9)
Model and Refinement Statistics				
resolution range (Å)				40.76–2.28
no. of reflections <sup>e</sup> (total)				13245
no. of reflections (test)				623
completeness (% of total)				99.6
$R_{\text{cryst}}^f$				0.207
$R_{\text{free}}^g$				0.246
Stereochemical Parameters				
bond length (Å)				0.015
bond angle (deg)				1.626
Wilson $B$ value ( $\text{\AA}^2$ )				48.72
ESU <sup>h</sup> based on $R_{\text{free}}$ value <sup>g</sup>				0.25 Å
no. of protein residues/atoms				191/1610
no. of solvent molecules				40
no. of ligand molecules				3 (2 Cl <sup>−</sup> , SO <sub>4</sub> )

<sup>a</sup> $\lambda 1$ – $\lambda 3$  were processed by XDS (version May 1, 2010);  $\lambda 4$  was processed by XDS (version March 15, 2012). <sup>b</sup>Values in parentheses are for the highest-resolution bin. <sup>c</sup>Members of a Friedel pair were counted separately. <sup>d</sup> $R_{\text{meas}} = \sum [N/(N-1)]^{1/2} \sum |I_i(hkl) - I(hkl)| / \sum \sum I_i(hkl)$ , where  $I_i$  is the scaled intensity of the  $i$ th measurement and  $|I_i|$  is the mean intensity for that reflection.<sup>63</sup> <sup>e</sup>Typically, the number of unique reflections used in refinement is slightly less than the total number that were integrated and scaled. Reflections are excluded because of systematic absences, negative intensities, and rounding errors in the resolution limits and cell parameters. <sup>f</sup> $R_{\text{cryst}} = \sum ||F_{\text{obs}}| - |F_{\text{calc}}|| / \sum |F_{\text{obs}}|$ , where  $F_{\text{calc}}$  and  $F_{\text{obs}}$  are the calculated and observed structure factor amplitudes, respectively. <sup>g</sup> $R_{\text{free}} = R_{\text{cryst}}$  but for 5.0% of the total reflections chosen at random and omitted from refinement. <sup>h</sup>Estimated overall coordinate error.<sup>64,65</sup>

polyacrylamide gel electrophoresis (SDS-PAGE), were pooled; His<sub>6</sub>-tagged TEV was added for His<sub>6</sub> tag cleavage, and dialysis was conducted simultaneously against TEV cleavage buffer [50 mM Tris (pH 8) and 500 mM NaCl] at 4 °C for 16 h. His<sub>6</sub> tag cleavage was verified by SDS-PAGE, and His<sub>6</sub>-tagged TEV, the cleaved His<sub>6</sub> tag, and any residual uncleaved GB1-ASC PYD were removed via a subtraction purification step over a gravity flow Ni<sup>2+</sup>-NTA column (Qiagen). The cleaved GB1-ASC PYD was further purified by size exclusion chromatography using a Superdex 75 26/60 column (GE Healthcare) equilibrated in NMR buffer. The purified protein was concentrated to 100 μM using centrifugal ultrafiltration (Amicon), flash-frozen, and stored at –80 °C.

**Crystallization and Data Collection.** Native and SeMet crystals were grown at 20 °C using vapor diffusion in sitting drops containing equal volumes of protein solution (1.0 μL of the purified NLRP4 PYD at 1.5 mg/mL in concentrated size exclusion buffer 1) and precipitant solution (0.1 μL of 0.2 M disodium tartrate and 2.2 M ammonium sulfate). Crystals formed after 4 days and were harvested, cryoprotected in paraffin oil, flash-frozen, and stored in liquid nitrogen. Diffraction data were collected at beamline BL14.1 at electron storage ring BESSY II (Berlin-Adlershof, Germany) operated by the Helmholtz-Zentrum Berlin (HZB)<sup>21</sup> and processed

using XDS.<sup>22</sup> One SeMet and one native crystal were used to determine the structure.

**Phasing and Refinement.** Data were phased in SHELX<sup>23,24</sup> using 10 sites to 3.5 Å from the SeMet data set, which yielded an interpretable electron density map. The model was refined against the 2.3 Å native data set. Iterative cycles of refinement and model building were conducted in Coot<sup>25</sup> and Phenix.<sup>26</sup> The final model was refined to  $R$  and  $R_{\text{free}}$  values of 0.207 and 0.246, respectively, at 2.28 Å resolution ( $R_{\text{free}}$  was calculated using 5% of the reflections randomly omitted from the refinement). Data collection, model, and refinement statistics are summarized in Table 1.

**Protein Data Bank (PDB) Entry.** Coordinates and structure factors were deposited in the RCSB Protein Data Bank as entry 4EWI.

**NMR Spectroscopy.** The interaction between the NLRP4 PYD (residues 1–110) and the ASC PYD (residues 1–94) was tested by NMR titration experiments. Two-dimensional (2D) <sup>1</sup>H–<sup>15</sup>N HSQC spectra of the [<sup>15</sup>N]NLRP4 PYD were acquired at 298 K on a Bruker Avance 500 MHz spectrometer equipped with a TCI HCN z-gradient cryoprobe and processed with Topspin 2.1 (Bruker). Data were analyzed using Cara (<http://cara.nmr.ch>); 10% D<sub>2</sub>O was added to all samples. A reference 2D <sup>1</sup>H–<sup>15</sup>N HSQC spectrum of the <sup>15</sup>N-labeled

Table 2. Summary of Structural and Electrostatic Similarity Statistics

PYD	PDB entry	Z score <sup>a</sup>	rmsd <sup>b,c</sup> (Å)	Is <sup>b,d</sup> (%)	L <sup>b,e</sup>	Qc <sup>b,f</sup> (%)	ED <sup>g</sup>	ref
NLRP1	1PNS	10.1	1.78	33	75	82	1.60	17
NLRP3	3QF2_A	12.9	1.79	34	83	91	1.44	16
NLRP7	2KM6	10.5	1.87	33	80	88	1.64	20
NLRP12	2L6A	10.7	1.82	40	81	89	1.52	19
ASC	1UCP	11.5	2.11	22	83	91	1.12	18
ASC2	2HM2	12.0	1.86	23	81	89	1.02	38

<sup>a</sup>Structural similarity search with the structure of the NLRP4 PYD using the DALI server.<sup>28</sup> <sup>b</sup>Values were calculated by TopMatch-web.<sup>29,30</sup> <sup>c</sup>Values were calculated by using all structurally equivalent Cα atoms. <sup>d</sup>Is gives the sequence identity of query and target in equivalent regions. <sup>e</sup>L (length of alignment) gives the number of residue pairs that are structurally equivalent. <sup>f</sup>Qc represents the relative cover of the query with respect to the target. Qc = 100 × L/Q<sub>n</sub>, where Q<sub>n</sub> is the length of the query sequence. <sup>g</sup>ED (electrostatic distance) calculated by PIPSA.<sup>35</sup>

NLRP4 PYD was recorded at a concentration of 50 μM in NMR buffer. Titration experiments were performed with a 2- or 3-fold molar excess of the unlabeled GB1-ASC L25A PYD in NMR buffer (25 μM [<sup>15</sup>N]NLRP4 PYD with 50 μM GB1-ASC-PYD or 16 μM [<sup>15</sup>N]NLRP4 PYD with 48 μM GB1-ASC PYD, respectively).

**Bioinformatics Analysis.** The sequence alignment of the NLRP4 PYD with the PYDs of NLRP1, -3, -7, and -12, ASC2, ASC was generated in Multalin,<sup>27</sup> and secondary structure comparison was completed using the on-line servers Dali<sup>28</sup> and TopMatch-web.<sup>29–31</sup> Protein–protein interactions between the two monomers making up the asymmetric unit were evaluated using ProtorP.<sup>32</sup> Structure visualization and analysis were performed in Pymol.<sup>33</sup> Electrostatic surface potentials were calculated using APBS<sup>34</sup> as part of the PIPSA (Protein Interaction Property Similarity Analysis) server<sup>35</sup> to generate quantitative comparisons between PYD electrostatic surface potentials.

**Co-Immunoprecipitation.** HEK293FT cells were seeded at 60% confluence in six-well tissue culture plates (Greiner). The following day, cells were cotransfected with 2 μg of plasmids encoding full-length Myc-tagged ASC and one of three truncated Flag-tagged NLRP4 constructs [NLRP4 PYD (residues 1–110), NLRP4 PYD+Linker (residues 1–162), and NLRP4 ΔLRR (residues 1–324)] using Transfectin (Bio-Rad) according to the manufacturer's protocol. The Flag-tagged Aim2 PYD (residues 1–96) was cotransfected as a positive control. On the day following transfection, cells were harvested and lysed in 200 μL of IP lysis buffer [50 mM Tris (pH 8.0), 150 mM NaCl, and 0.5% Nonidet P-40] supplemented with protease inhibitor (Sigma Aldrich). After centrifugation, the clarified lysate from each sample was subjected to overnight immunoprecipitation at 4 °C with anti-Myc antibodies (AbD Serotec) immobilized on G-Sepharose (Invitrogen). The immunoprecipitated complexes were washed four times with IP lysis buffer and, along with a 5% total cell extract control, resolved via 12% SDS-PAGE, transferred to nitrocellulose membranes (Whatman), and analyzed by immunoblotting using anti-Myc (AbD Serotec) or anti-Flag (Sigma) primary antibodies and AP-labeled secondary antibodies (Santa Cruz Biotechnology). Nitro-blue tetrazolium (NBT) and 5-bromo-4-chloro-3-indolyl phosphate (BCIP) (Roche) were used to augment the signal for protein detection.

**Yeast Two-Hybrid Analysis.** The two-hybrid experiments were performed with MATCHMAKER GAL4 Two-Hybrid System 3 (Clonetech) following the manufacturer's instructions. In summary, the NLRP4 PYD, NLRP4 PYD+Linker, and ASC PYD were each inserted into the pGBKT7 and pGADT7 fusion vectors encoding a reporter GAL4 DNA-binding

domain (BD) and an activation domain (AD), respectively, whose proximity is necessary for producing a signal. *Saccharomyces cerevisiae* reporter strain Y2HGold (Clonetech) was cotransformed with either the pGADT7-NLRP4 PYD (bait protein) or the pGADT7-NLRP4 PYD+Linker and the pGBKT7-ASC PYD (library protein) or the pGADT7-ASC PYD (bait protein) and the pGBKT7-NLRP4 PYD or the pGBKT7-NLRP4 PYD+Linker (library protein) using a small-scale lithium acetate/single-stranded carrier DNA/polyethylene glycol (LiAc/ss-DNA/PEG) transformation protocol.<sup>36</sup> Transformed yeast cells were resuspended in sterile water and spotted onto SD/-Leu/-Trp dropout medium to assess transformation efficiency and onto SD/-Ade/-His/-Leu/-Trp selection medium to test for potential interactions. Plates were incubated for 4–5 days at 30 °C. To rule out self-activation of reporter genes, all fusion constructs were tested for their ability to activate transcription of the GAL4 reporter or to associate with either the GAL4 BD or GAL4 AD. Cotransformation of the pGBKT7-ASC PYD and pGADT7-Aim2 PYD (residues 1–96) served as a positive interaction control.<sup>37</sup>

## RESULTS

**Bioinformatics Analysis of the NLRP4 PYD.** The human genome contains 14 NLRP proteins {NLRP1–NLRP14 [HUGO Gene Nomenclature Committee (HGNC, <http://www.genenames.org>)].} Structural information is available for the PYDs of human NLRP1, NLRP3, NLRP7, NLRP12, ASC, ASC2 and murine NLRP10 (PDB entry 2DO9).<sup>16–20,38</sup> A sequence homology search using the FFAS server<sup>39</sup> shows a high degree of conservation between NLRPs, with the highest level of sequence identity (50%) observed between the NLRP4 PYD and the NLRP14 PYD (NCBI entry NP\_789792.1). In addition, the sequence of the NLRP4 PYD is 40% identical with that of the NLRP12 PYD (PDB entry 2L6A),<sup>19</sup> 34% identical with that of the NLRP3 PYD (PDB entry 3QF2),<sup>16</sup> 33% identical with that of the NLRP1 PYD (PDB entry 1PNS),<sup>17</sup> and 33% identical with that of the NLRP7 PYD (PDB entry 2KM6)<sup>20</sup> (Table 2). Furthermore, the sequence of NLRP4 PYD is 22% identical with that of the adaptor protein ASC PYD (PDB entry 1UCP)<sup>18</sup> and 23% identical with that of ASC2 (also known as POP1) (PDB entry 2HM2),<sup>38</sup> the dominant-negative modulator of ASC.<sup>40</sup>

**The NLRP4 PYD is a Monomer in Solution.** The NLRP4 PYD (residues Met1–Leu110) was expressed in *E. coli* and purified to homogeneity. As verified by size exclusion chromatography, the NLRP4 PYD exists as a monomer in solution (Figure S1A of the Supporting Information). To further characterize NLRP4 PYD multimerization in solution, we placed the <sup>15</sup>N-labeled NLRP4 PYD in a weakly reducing

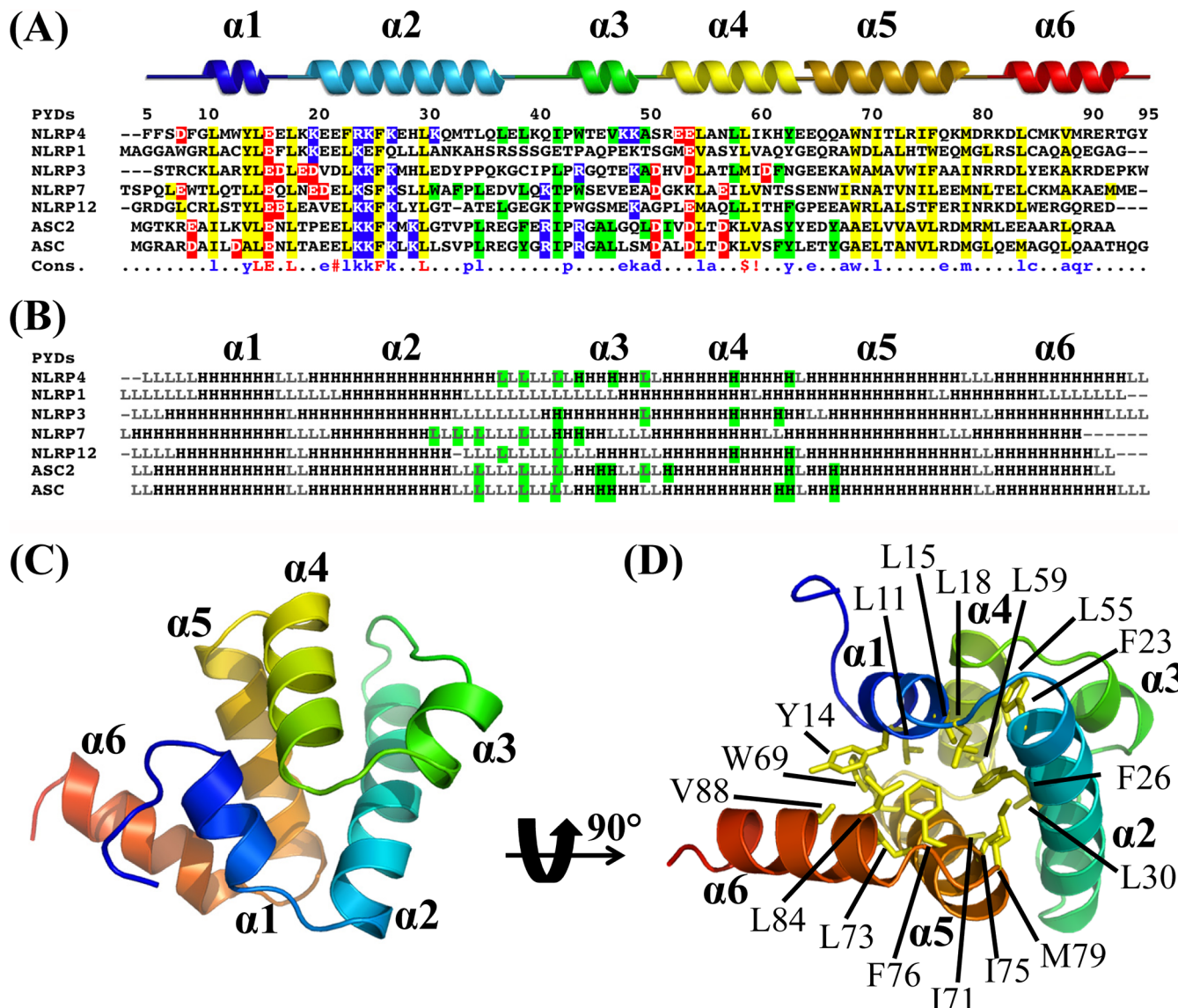


**Figure 1.** Structural characterization of the NLRP4 PYD. (A) Primary sequence alignment of the NLRP4 PYD and the PYDs of NLRP1, NLRP3, NLRP7, NLRP12, ASC2, and ASC. The six NLRP4 PYD  $\alpha$ -helices, illustrated above the sequence, are color-coded from the N-terminus (blue) to the C-terminus (red) and labeled from  $\alpha_1$  to  $\alpha_6$ . Hydrophobic core-forming residues are highlighted in yellow; residues forming the second hydrophobic cluster to stabilize helix  $\alpha_3$  are highlighted in green. Positively and negatively charged residues responsible for PYD surface charges are colored blue and red, respectively. Consensus indicates residues that are >90% identical (red) and 50% identical (blue) (! is either Ile or Val; \$ is either Leu or Met; # is either Asp or Glu). (B) Comparison of the secondary structural elements of the NLRP4 PYD and the PYDs of NLRP1, NLRP3, NLRP7, NLRP12, ASC2, and ASC (H, helix; L, loop). Helices are labeled from  $\alpha_1$  to  $\alpha_6$ . (C) Cartoon representation of the NLRP4 PYD with the six  $\alpha$ -helices colored from the N-terminus (blue) to the C-terminus (red) and labeled from  $\alpha_1$  to  $\alpha_6$ . (D) The NLRP4 PYD (rotated by 90° along the  $x$ -axis relative to the view in panel (C)) is stabilized by an extensive (hydrophobic core residues are labeled and shown as yellow sticks).

buffer (0.5 mM TCEP; the NLRP4 PYD has one cysteine, Cys85), waited several days to allow for any dimerization to occur, and recorded a 2D  $^1\text{H}$ - $^{15}\text{N}$  HSQC NMR spectrum. The outstanding quality of the spectrum (Figure S1B of the Supporting Information) is typical for a small 13.9 kDa protein, indicating that the  $^{15}\text{N}$ -labeled NLRP4 PYD exists as a monomer after several days under weakly reducing conditions.

The NLRP4 PYD in NMR buffer cannot be concentrated using Amicon Ultra centrifugal filters (Millipore), as it readily precipitates. This phenomenon has been observed in other NLR effector domains [NLRP1<sup>17</sup> and NLRC5 (unpublished data)] and seems to be a common feature of this protein subfamily. We found concentration by evaporation, which increases the concentration of all sample components (i.e.,

protein, salt, and TCEP), to be more efficient, allowing the NLRP4 PYD to reach a concentration of 3 mg/mL. Crystallization was conducted using the sitting drop vapor diffusion method. Crystals appeared within 4 days, diffracted to 2.3 Å, and were indexed in space group  $P3_21$ , with two molecules in the asymmetric unit. Because of heavy twinning (45%) (phenix.xtriage),<sup>26</sup> it was impossible to determine the structure using the initial SeMet data sets. However, several rounds of crystallization optimization combined with diffraction screening of 50 SeMet and 15 native crystals allowed one SeMet and one native crystal with <3% twinning to be identified that yielded quality data suitable for structure determination.

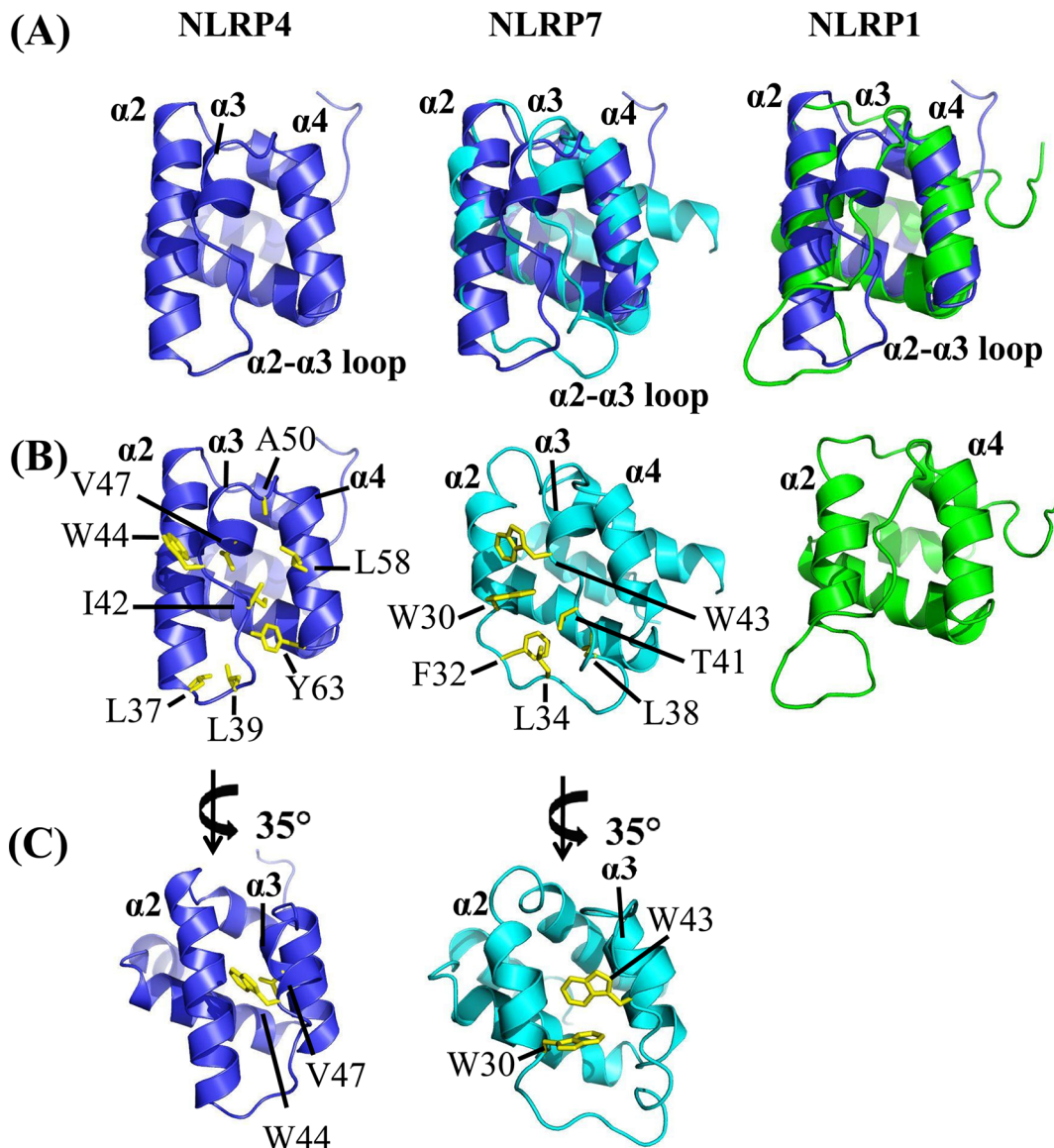


**Figure 2.** Structural comparison of the NLRP4 PYD with the PYDs of NLRP7 and NLRP1. (A) Superposition of the NLRP4 PYD (blue) on the NLRP7 PYD (cyan) and the NLRP1 PYD (green). (B) Residues that stabilize helix  $\alpha_3$  in the NLRP4 PYD and the NLRP7 PYD are labeled and shown as yellow sticks. Corresponding hydrophobic residues are missing in the NLRP1 PYD. (C) Trp44 in the NLRP4 PYD is structurally conserved in the NLRP7 PYD.

**Crystal Structure of the NLRP4 PYD.** The final model includes two NLRP4 PYD monomers (residues Phe5–Tyr95 in chain A and Phe5–Gly94 in chain B), one sulfate ion, two chloride ions, and 40 water molecules in the asymmetric unit. No electron density was observed for the N- and C-termini (residues Met1–Ser4 and Thr96–Leu110 in chain A and Met1–Ser4 and Tyr95–Leu110 in chain B). The Matthews coefficient ( $V_m$ ) for the NLRP4 PYD is  $2.50 \text{ \AA}^3/\text{Da}$ , and the estimated solvent content is 51%. The Ramachandran plot shows that 99.4% of the residues are in the allowed regions.

The crystal structure of the NLRP4 PYD adopts a typical death domain fold (Figure 1). Six  $\alpha$ -helices ( $\alpha_1$ – $\alpha_6$ ) are tightly packed around a central hydrophobic core [formed by Leu11, Tyr14, Leu15, Leu18, Phe23, Phe26, Leu30, Leu55, Leu59, Trp69, Ile71, Leu73, Ile75, Phe76, Met79, Leu84, and Val88 (Figure 1A,C,D)] and form an antiparallel  $\alpha$ -helical bundle. This well-defined hydrophobic core, which defines the death domain fold, is conserved throughout the entire DD super-

family.<sup>19,41</sup> The six ordered  $\alpha$ -helices of the NLRP4 PYD are connected by loops ranging from one to five amino acids in length (Figure 1B,C). The loops connecting helices  $\alpha_1$  (Gly10–Glu16) to  $\alpha_2$  (Lys20–Gln36),  $\alpha_3$  (Trp44–Lys49) to  $\alpha_4$  (Arg52–Tyr63), and  $\alpha_5$  (Glu65–Lys78) to  $\alpha_6$  (Lys82–Thr93) are each three amino acids in length, while the  $\alpha_2$ – $\alpha_3$  loop is composed of five amino acids that are disordered. Helices  $\alpha_4$  and  $\alpha_5$  are linked by only a single residue, Glu64, making this linker structurally constrained, which accounts for its outlier position in the Ramachandran plot.

**Homodimeric Interface in the NLRP4 PYD Crystallographic Dimer.** Two NLRP4 PYD monomers (chains A and B) form a dimer in the asymmetric unit, which are related by a pseudo-2-fold axis at the dimerization interface. The interface buries  $2252 \text{ \AA}^2$  of solvent-accessible surface area (SASA), which corresponds to a 17.83% burial of the SASA of each monomer<sup>32</sup> and is thus in the range of biologically relevant protein–protein interfaces. The NLRP4 dimer interface is

comprised of both electrostatic and hydrophobic interactions. Contacts are formed by the side chains of Phe9\_A (chain A) with Leu73\_B (chain B), Ile60\_A with Ile60\_B, Gln66\_A with the main chain of Phe9\_B, and Lys87\_A with the main chain of Glu91\_B (Figure S2 of the Supporting Information). Because of the pseudo-2-fold axis, the reverse interactions (i.e., Phe9\_B with Leu73\_A, etc.) are also present.

While a dimer was observed in the crystal, SEC and NMR data show that the NLRP4 PYD is monomeric in solution. Interestingly, a similar behavior has been observed for the CARD of NLRC1 (also termed CARD1 or Nod1).<sup>42</sup> Specifically, two NMR structures clearly show that the NLRC1 CARD forms a monomer in solution (ref 43 and PDB entry 2DBD), while two crystal structures<sup>42,44,45</sup> show that the NLRC1 CARD forms disulfide-linked dimers. Interestingly, NLRP4 PYD dimerization does not appear to be a result of a disulfide bond between Cys85 residues from each monomer, as Cys85 in each monomer is distal from the dimerization interface, with the corresponding sulfur atoms more than 26 Å apart. Taken together, our data and other available PYD and CARD data suggest that dimer formation (either via disulfide bonds or, in our case, via other protein–protein interactions) is likely induced by crystal packing.

However, PYD or CARD dimerization may still be necessary for some aspects of PYD or CARD function. Homotypic interactions between PYDs (in the case of inflammasomes) and CARDs (in apoptosomes and some inflammasomes) are complex, and even dynamic in nature. The ability of PYDs and CARDs to easily make the transition between the monomeric and dimeric states might be important for their function, such as stabilization of the inflammasome and apoptosome signaling platforms, respectively, thereby improving the efficacy of downstream signaling.<sup>46</sup> It should be noted that Cys85 in helix  $\alpha$ 6 of the NLRP4 PYD is conserved in NLRP1, -7, -8, -11, -13, and -14, and although no cysteine mutation with a discernible phenotype has been reported so far, future studies are necessary to investigate the physiological relevance, if any, of disulfide-linked PYDs.

**Variation among NLR PYDs.** The death domain superfamily, which includes the death domain (DD), the death effector domain (DED), the CARD, and the PYD subfamilies, is characterized by six antiparallel  $\alpha$ -helices packed in a Greek key topology.<sup>47</sup> Recently, we used the structures of the PYDs of NLRP7 and -12 to identify the key conserved residues necessary for forming the conserved hydrophobic core of DD family members.<sup>19</sup> On the basis of the aforementioned structural comparisons, we expected the hydrophobic core of the NLRP4 PYD to be formed by Leu11, Tyr14, Leu15, Leu18, Phe23, Phe26, Leu30, Leu55, Leu59, Trp69, Ile71, Leu73, Phe76, Met79, and Leu84, which are in perfect agreement with the core residues seen in our crystal structure (residues highlighted in yellow in Figure 1A,D).<sup>19</sup>

The NLRP4 PYD was superimposed onto the structures of several PYDs using the TopMatch-web server<sup>29–31</sup> (Figure 2), which revealed high levels of structural similarity between all analyzed PYDs [pairwise rmsds of ~1.8 Å (Table 2)]. However, the NLRP4 PYD and NLRP1 PYD showed relatively subtle but significant differences from the NLRP7 PYD. Namely, both the NLRP4 PYD and the NLRP1 PYD possess the shortest  $\alpha$ 1 helix as well as the longest  $\alpha$ 2 and  $\alpha$ 6 helices (Figures 1B and 2A). Given the high degree of conservation of tertiary and secondary structural elements of PYDs, their evolutionary relationship was investigated using TraceSuite II.<sup>48</sup> The

phylogenetic tree is shown in Figure S3 of the Supporting Information and assigns two large branches. One branch consists of the adaptor ASC and its inhibitor ASC2, while the second branch groups the receptor PYDs of NLRP1, -3, -4, -7, and -12.

The most striking difference seen in the NLRP4 PYD, when compared to NLRP1 and NLRP7 PYDs, is the length of helix  $\alpha$ 3 and the  $\alpha$ 2– $\alpha$ 3 connecting loop (Figure 2A,B). In the NLRP4 PYD, helix  $\alpha$ 3 is composed of two turns and is stabilized by Leu37, Leu39, and Ile42 from the  $\alpha$ 2– $\alpha$ 3 connecting loop, Trp44 and Val47 from helix  $\alpha$ 3, Ala50 from the  $\alpha$ 3– $\alpha$ 4 connecting loop, and Leu58 and Tyr63 form helix  $\alpha$ 4 (Figures 1A,B and 2B). This hydrophobic cluster, which is centered on helix  $\alpha$ 3 and the  $\alpha$ 2– $\alpha$ 3 connecting loop, is conserved in NLRP3, NLRP7, and ASC PYDs and, to a lesser extent, in the NLRP12 PYD and ASC2 (where helix  $\alpha$ 3 is only a single turn helix). In contrast, the NLRP1 PYD completely lacks hydrophobic residues in helix  $\alpha$ 3 and the  $\alpha$ 2– $\alpha$ 3 connecting loop that are required for stabilization of these structural elements. Instead, the NLRP1 PYD forms a long unstructured linker between helices  $\alpha$ 2 and  $\alpha$ 4.<sup>17</sup> Lastly, residue Trp44 of the NLRP4 PYD is structurally conserved in NLRP7 and NLRP12 PYDs. Both Trp43 (NLRP7 PYD) and Trp44 (NLRP4 PYD) form a hydrophobic stacking interaction that stabilizes helix  $\alpha$ 3 (Figure 2C). In contrast, Trp45 of the NLRP12 PYD is surface-exposed and mediates a protein–protein interaction with the FAF-1 UBA domain.<sup>19</sup>

The difference in helix  $\alpha$ 3 between the various PYD structures is important, as it has been suggested that a disordered helix  $\alpha$ 3 that becomes fully folded only upon binding to downstream partners is a common feature in PYDs and thus was considered to have a crucial role in the protein–protein interactions required for inflammasome signaling.<sup>17,20,49</sup> In fact, this highly variable region, along with the variable  $\alpha$ 2– $\alpha$ 3 connecting loop, was shown to play a key role in guiding homotypic as well as heterotypic PYD binding interactions.<sup>19,50</sup> While it is extremely likely that all other PYDs with unknown structures contain the well-established hydrophobic core formed by helices  $\alpha$ 1,  $\alpha$ 2, and  $\alpha$ 4– $\alpha$ 6, we can also expect to see increasing diversity in the conformations of helix  $\alpha$ 3 and the  $\alpha$ 2– $\alpha$ 3 connecting loop, like those seen in the NLRP4 PYD, as more PYD structures are determined.

**Comparison of the PYD Family Reveals Distinct Electrostatic Surfaces.** It has been well established that oppositely charged electrostatic surface potentials (ESPs) have a vital role in the formation of homotypic death domain interactions. Recently reported structures of the PIDDosome, the FAS–FADD complex, and the Apaf-1–Caspase-9 complex highlighted the importance of charged surfaces in homotypic DD and CARD interactions.<sup>51–53</sup> A similar electrostatic interaction mechanism was described for the homotypic PYD interaction between the ASC PYD and ASC2. Specifically, a large positively charged surface on ASC2 (formed by Lys21, Lys22, Lys24, Lys26, Arg38 and Arg41 from helices  $\alpha$ 2 and  $\alpha$ 3) interacts with a complementary negatively charged surface on the ASC PYD [formed by residues Asp6, Asp10, Glu13, Asp48, Asp51, and Asp54 from helices  $\alpha$ 1 and  $\alpha$ 4 (residues highlighted in blue and red in Figures 1A and 3)].<sup>50</sup>

Thus, we analyzed the ESP of the NLRP4 PYD, which showed that the NLRP4 PYD also possesses two distinctly charged surfaces. The NLRP4 PYD has a prominent positively charged region spanning helices  $\alpha$ 2 and  $\alpha$ 3, as well as a weaker negatively charged surface consisting of Asp8 and Glu16 from

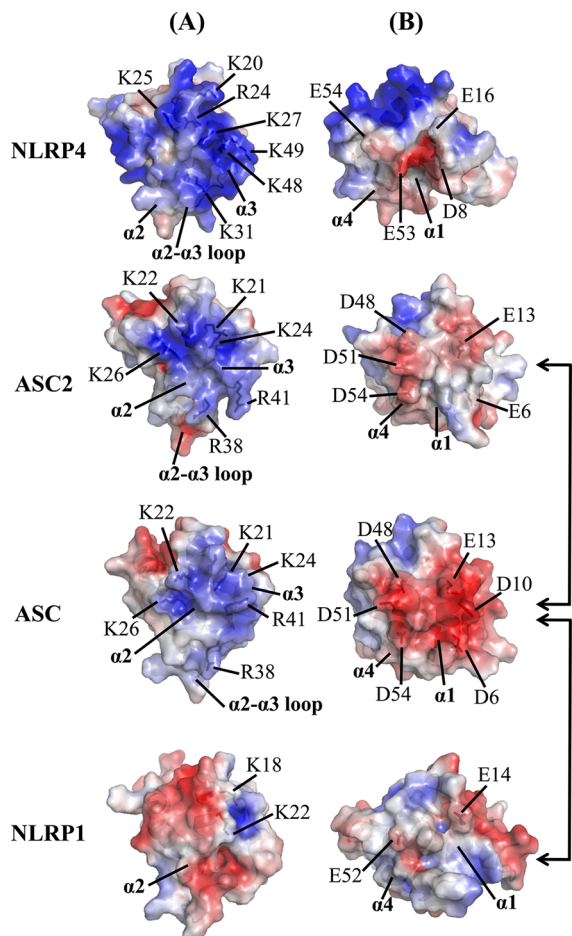


**Figure 3.** Electrostatic surface potentials of the NLRP4 PYD compared to ASC2 and the PYDs of ASC and NLRP1. The electrostatic potentials (ESPs) of the two interaction surfaces formed by helices  $\alpha_2$  and  $\alpha_3$  and helices  $\alpha_1$  and  $\alpha_4$  are mapped on the solvent-accessible surface of the identically oriented PYDs from NLRP4, NLRP1, ASC, and ASC2. The color scale varies from red (negative ESP) to blue (positive ESP). Residues responsible for these charges are labeled on each structure. Arrows indicate previously experimentally detected direct homotypic PYD interactions.

helix  $\alpha_1$  and Glu53 and Glu54 from helix  $\alpha_4$ , which is especially similar to ASC2. Figure 3 illustrates the electrostatic surfaces of the NLRP4 PYD and the PYDs of NLRP1, ASC, and ASC2. Electrostatic similarity calculations performed by the PIPSA server<sup>35</sup> showed that the NLRP4 PYD is most similar to ASC2 (electrostatic distance of 1.02; a distance of 0 indicates the electrostatic surface potentials are identical, while a score of 2 indicates they are completely opposite) followed by the ASC PYD (electrostatic distance of 1.12), NLRP3 PYD (electrostatic distance of 1.44), NLRP12 PYD (electrostatic distance of 1.52), NLRP1 PYD (electrostatic distance of 1.60), and NLRP7 PYD (electrostatic distance of 1.64).

The significant electrostatic similarity of NLRP4 and ASC2 is based on a highly positively charged ESP encompassing Lys20, Arg24, Lys25, Lys27, and Lys31 on helix  $\alpha_2$  and Lys48 and Lys49 on helix  $\alpha_3$  (Figure 3). Currently, no other NLRP PYD has been shown to possess a similarly extensive positively charged surface. In other NLRP PYD structures, this surface is either mostly negatively charged (NLRP1 PYD), slightly positively charged with a prominent hydrophobic patch

(NLRP12 PYD), or slightly negatively charged with a significant hydrophobic patch (NLRP7 and NLRP3 PYDs).

The inflammasome receptors NLRP1 and NLRP3 were shown to interact with ASC, leading to the formation of the inflammasome signaling platform.<sup>19,20,54,55</sup> Interestingly, the ESPs of NLRP1 and NLRP3 are different, highlighting that the electrostatic nature of these protein–protein interactions might have been overemphasized. Specifically, the NLRP3 PYD is mainly negatively charged and thus was proposed to interact with the positively charged surface of the ASC PYD, while not competing with ASC2 for the negatively charged surface of the ASC PYD.<sup>50</sup> The electrostatic surface of the NLRP1 PYD also differs from those of the NLRP3 PYD and ASC2. Taken together, this indicates that homotypic PYD–PYD interactions, which were previously thought to be due to the attraction between oppositely charged surfaces, are likely more complex. This is further confirmed by our observation that both the NLRP7 PYD and the NLRP12 PYD have negatively charged surfaces that are comparable to that of NLRP3, but unlike NLRP3, they are unable to interact with ASC.<sup>19,20</sup>

**The NLRP4 PYD Does Not Interact Directly with the ASC PYD.** Interestingly, the NLRP4 PYD has a positively charged surface that is very similar to that of ASC2. In ASC2, this positively charged surface is responsible for its interaction with the ASC PYD (Figure 3).<sup>50</sup> Furthermore, NLRP4 was shown to form heterotypic oligomers with the inflammasome-forming receptors NLRP3 and NLRC4 via NACHT domain interactions.<sup>15,56</sup> This raises the question of whether the NLRP4 PYD also interacts with the ASC PYD, thus leading to caspase 1 and IL-1 $\beta$  activation.

On the basis of these observations, we tested for an interaction between the NLRP4 PYD and the ASC PYD via NMR chemical shift perturbation (CSP) analysis. Specifically, we recorded a 2D heteronuclear  $^1\text{H}$ – $^{15}\text{N}$  HSQC spectrum of the  $^{15}\text{N}$ -labeled NLRP4 PYD and then added the unlabeled ASC PYD in a 2- and 3-fold molar excess to the  $^{15}\text{N}$ -labeled NLRP4 PYD sample (the limited solubility of these proteins did not allow for higher ratios to be tested; throughout this work, the solubility-enhancing L25A mutant of the ASC PYD was used for all NMR measurements). No CSPs were detected, indicating that there is no direct interaction between the PYDs of NLRP4 and ASC (Figure S4 of the Supporting Information). It should be noted that NMR titration experiments were conducted at pH 7.2 such that the environment more closely resembled that of the cell, as previous reports indicated that death domain interactions are affected by low pH<sup>52</sup> (previous *in vitro* interaction experiments using the ASC PYD were conducted at pH 4.5, due to the insolubility of the ASC PYD at physiological pH). As the recombinant ASC PYD is expressed insolubly in bacterial cells, purification requires denaturation of inclusion bodies and protein refolding. Using a GB1 solubility tag, we succeeded in expressing and purifying the soluble, monomeric ASC PYD (confirmed by SEC). The increased solubility and stability of the GB1-tagged construct allowed for the acquisition of NMR data at physiological pH. GB1 is a widely used solubility-enhancing tag for NMR studies that has been successfully used for structural and interaction studies of ~30 proteins that represent a broad variety of structural topologies and biological functions.<sup>57</sup> The N-terminal GB1 tag is joined to the ASC PYD via a four-amino acid linker, which is sufficiently long (~12 Å) so as not to affect the three-dimensional structure of the ASC PYD. To confirm this, we superimposed the 2D  $^1\text{H}$ – $^{15}\text{N}$  HSQC spectra of the untagged

and GB1-tagged <sup>15</sup>N-labeled ASC PYD (acquired under identical buffer conditions). Figure S5 of the Supporting Information shows that both spectra overlap very well, confirming that the GB1-tagged ASC PYD adopts a structure nearly identical to that of the untagged ASC PYD. Only a small number of minor differences in the chemical shifts of GB1-tagged and untagged ASC PYDs are observed for residues in helix  $\alpha 1$ , which is closest to the N-terminal GB1 tag, and for a few residues in helices  $\alpha 4$  and  $\alpha 5$ , likely the result of side chain interactions with the nearby helix  $\alpha 1$ . Importantly, the  $\alpha 2-\alpha 3$  surface and helix  $\alpha 6$  of the ASC PYD are unaffected by the presence of the GB1 tag. In summary, we developed a new approach that uses the GB1-ASC PYD to test homo- and heterotypic PYD interactions at physiological pH and used it to show that there is no interaction between the NLRP4 PYD and the ASC PYD.

We also tested for an interaction between NLRP4 and the ASC PYD using cellular assays. First, co-immunoprecipitation assays were performed in HEK 293FT cells with Myc-tagged ASC and several truncated Flag-tagged NLRP4 constructs (Figure S6A of the Supporting Information). Because the ligand for NLRP4 activation is unknown, truncated constructs including the NLRP4  $\Delta$ LRR (NLRP4 lacking the LRR domain), NLRP4 PYD+Linker, and NLRP4 PYD were used to avoid a misleading result from an autoinhibited receptor that is unable to bind the downstream signaling partner. However, in agreement with the NMR studies, we were not able to detect an interaction between NLRP4 and ASC by co-immunoprecipitation (Figure S6A of the Supporting Information). The previously reported Aim2 PYD-ASC PYD interaction was used as a positive control. Lastly, we performed a yeast two-hybrid analysis of the NLRP4 PYD and NLRP4 PYD+Linker with the ASC PYD, which again confirmed the NMR and co-immunoprecipitation results (Figure S6B of the Supporting Information).<sup>37</sup>

Thus, although the NLRP4 PYD has distinct and oppositely charged surface patches that were originally thought to be necessary for homotypic PYD interactions, we were not able to detect a direct interaction between the NLRP4 PYD and the ASC PYD. These findings are in agreement with the observation that NLRP4 has no effect on IL-1 $\beta$  activation<sup>14,15,38</sup> and show that other factors must play a vital role in forming these interactions. Furthermore, they are in line with the previously reported importance of hydrophobic residues in CARD-CARD homotypic interactions<sup>59</sup> as well as a PYD heterotypic interaction recently reported between the NLRP12 PYD and FAF-1.<sup>19</sup>

## ■ DISCUSSION

PYDs are the most abundant members of the DD superfamily, and it has become apparent that they have an essential role in the control of signaling in immune and apoptotic pathways.<sup>1,47</sup> During the past 5 years, numerous PYD structures have been reported, which have resulted in detailed analyses of both the structural and, in the case of NMR structures, dynamic parameters that control PYD activity and specificity.<sup>16-20,38</sup> While the structural and dynamics differences between PYDs are more numerous than the similarities, work on the signaling adaptor protein ASC and its inhibitor ASC2 showed the importance of electrostatic complementarity between PYD domains for their interactions.<sup>50,60</sup> Similar results were reported for CARD-CARD and DD-DD interactions.<sup>51,52,59</sup>

Here, we report the three-dimensional crystal structure of the NLRP4 PYD at 2.3 Å resolution. The NLRP4 PYD adopts a typical DD fold with six  $\alpha$ -helices that are arranged in an antiparallel helical bundle around a highly conserved hydrophobic core. This hydrophobic core was previously established on the basis of our work on multiple NLRP PYD domains.<sup>19,20</sup> Hydrophobic residues also play a decisive role in stabilizing the conformation of helix  $\alpha 3$  and the  $\alpha 2-\alpha 3$  connecting loop relative to the rest of the domain, as readily seen in the structures of the PYDs from NLRP3, NLRP7, NLRP12, and now NLRP4. The only outlier is the NLRP1 PYD, in which helix  $\alpha 3$  does not exist and the  $\alpha 2-\alpha 3$  connecting loop is exceedingly dynamic, as probed by fast time scale autocorrelated relaxation measurements.<sup>17</sup> This is important, as the surface formed by helix  $\alpha 3$  and the  $\alpha 2-\alpha 3$  connecting loop has been identified as an important protein-protein interaction site for PYDs, and thus, differences in this region are likely the driving force for differential binding and selectivity among PYDs.

Interestingly, in the NLRP4 PYD, the surface electrostatics of helix  $\alpha 3$  and the  $\alpha 2-\alpha 3$  loop region are highly similar to those of the ASC PYD and ASC2. A model of the ASC PYD-ASC2 complex showed that the positive ESP of ASC2 interacts with the negative ESP of the ASC PYD.<sup>50</sup> Thus, we tested for an interaction between the NLRP4 PYD and the ASC PYD using a variety of in vitro and in vivo tools. Significantly, to perform in vitro studies with the ASC PYD under biologically relevant conditions, it was necessary to develop a novel construct of the ASC PYD that was stable at physiological pH. This is because, until this work, the heterologously expressed ASC PYD had only been isolated and refolded from inclusion bodies and was only stable at acidic pH values. By fusing the ASC PYD to GB1, a small highly soluble protein domain, we were able to express soluble ASC PYD that, once purified, is stable at physiological pH (i.e., 7.2). This is critical, as previous reports showed that homotypic PYD-PYD interactions are very sensitive to pH, with optimal interaction conditions occurring at physiological pH.<sup>61</sup> Thus, the GB1-ASC PYD construct is an exciting new tool for research in the NLRP field.

Interestingly, using both in vitro CSP measurements and in vivo pull-down studies, we were not able to detect a direct interaction between the NLRP4 PYD and ASC PYD. Overlap of the three-dimensional structure of the NLRP4 PYD, the ASC PYD, and ASC2 allows for structural comparisons of the Arg and Lys residues that are responsible for the formation of the positively charged surface. Notably, the NLRP4 PYD has a novel second positively charged surface, which is formed by residues Arg74 and Lys78 on helix  $\alpha 5$  and Lys82 on helix  $\alpha 6$  (Figure 4). This is interesting, as the  $\alpha 5-\alpha 6$  loop and helix  $\alpha 6$  are proposed to engage in homotypic type II interactions that occur within large signaling platforms, as was described for the homotypic DD interaction within the PIDDosome.<sup>41,47,51</sup>

Our structure of the NLRP4 PYD, especially in the context of the PYD family, further illustrates that the electrostatic surface distribution varies widely among PYDs. Thus, it is increasingly apparent that individual PYDs most likely have distinct interaction partners.<sup>19,62</sup> Furthermore, we have also shown that NLRP4 differs from ASC-binding PYDs in several important aspects and thus likely functions in an ASC-independent manner. Our structural analysis and CSP experiments also show that electrostatic interactions might not be as important as previously assumed for death domain fold protein interactions. In agreement with our data, previous reports

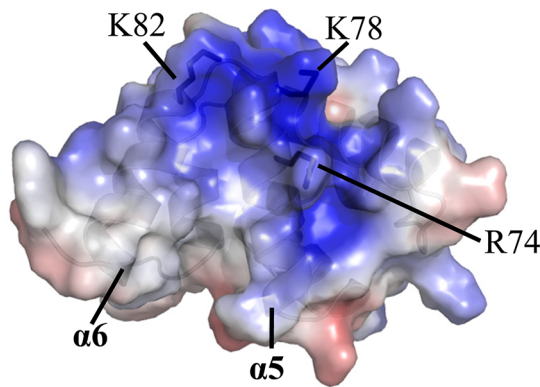


**Figure 4.** NLRP4 PYD showing an additional positive patch. The electrostatic potentials of helices  $\alpha_5$  and  $\alpha_6$  are mapped onto the solvent-accessible surface of the NLRP4 PYD. Residues Arg74, Lys78, and Lys82, form this positively charged surface.

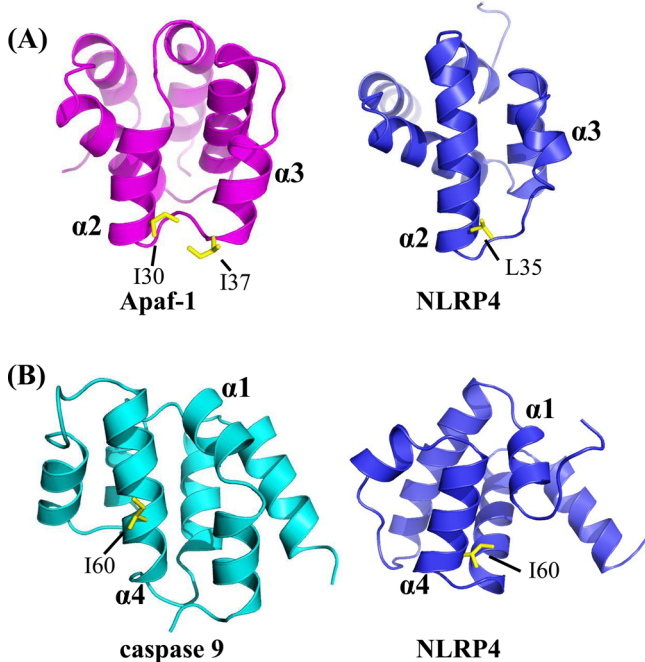


**Figure 5.** Comparison of the NLRP4 PYD with the Apaf-1 CARD and the caspase 9 CARD. Residues (yellow sticks) that mediate a hydrophobic interaction between the Apaf-1 CARD (magenta) and the caspase 9 CARD (cyan) are also surface-exposed in the NLRP4 PYD (blue).

highlighted the importance of hydrophobic interactions for the homotypic DD. Indeed, as shown in Figure 5, the CARD domains of Apaf-1 and caspase 9 share many structural features with the NLRP4 PYD. This comparison allowed us to identify hydrophobic residues that are important for the CARD–CARD interaction between Apaf-1 and caspase 9 within the NLRP4 PYD. Specifically, Ile30 in the Apaf-1 CARD is located at the last turn of helix  $\alpha_2$ , which structurally aligns with Leu35 in the NLRP4 PYD (Figure 5A). Furthermore, Ile60 in caspase 9 structurally aligns with Ile60 in the NLRP4 PYD which is, however, shifted by one turn in helix  $\alpha_4$  (Figure 5B).

Taken together, our earlier findings describing the Pyrin domain fold and stability, combined with our current work, have significantly contributed to the characterization of PYDs and their function. The findings described here suggest that the

generally accepted electrostatic model of PYD–PYD interaction specificity is incomplete and that additional factors, such as dynamics and hydrophobic interactions, also likely play an important role in these interactions.

## ASSOCIATED CONTENT

### Supporting Information

Figures of SEC chromatograms, NMR spectra, the crystallographic dimer, phylogenetic tree, co-immunoprecipitation, and Y2H results. This material is available free of charge via the Internet at <http://pubs.acs.org>.

## AUTHOR INFORMATION

### Corresponding Author

\*K.D.: Fachbereich Biologie, Universität Konstanz, D-78457 Konstanz, Germany; phone, +49 7531 88-4049; e-mail, kay.diederichs@uni-konstanz.de. W.P.: Department of Molecular Pharmacology, Physiology and Biotechnology, Brown University, Providence, RI 02903; phone, (401) 863-6084; e-mail, wolfgang\_peti@brown.edu.

### Funding

This research was funded by the Austrian Science Fund (FWF) under Project W1213 (to C.E.), Marie Curie Excellent Grant MCEXT033534 from the European Community to J.W., Erwin-Schrödinger Postdoc Fellowships from the Austrian Science Fund to S.P. (J3173 - N17) and M.P. (J 2956-B12), and National Institutes of Health Grants R01-AI-56324 to J.C.R. X-ray data collection was performed at the electron storage ring BESSY II of the Helmholtz-Zentrum Berlin fuer Materialien und Energie (Berlin, Germany) and was supported by the European Community's Seventh Framework Program (FP7/2007-2013) under Grant 226716.

### Notes

The authors declare no competing financial interest.

## ACKNOWLEDGMENTS

We thank Dr. Eva de Alba (Centro de Investigaciones Biológicas, Consejo Superior de Investigaciones Científicas, Madrid, Spain) for sharing the ASC plasmid.

## ABBREVIATIONS

rmsd, root-mean-square deviation; NLR, nucleotide-binding domain and leucine-rich repeat-containing proteins; LRR, leucine-rich repeats; DD, death domain; PYD, pyrin domain; CARD, caspase activation and recruitment domain; ASC, apoptosis-associated speck-like protein containing a CARD; ESP, electrostatic surface potential; NMR, nuclear magnetic resonance.

## REFERENCES

- (1) Kersse, K., Bertrand, M. J., Lamkanfi, M., and Vandenberghe, P. (2011) NOD-like receptors and the innate immune system: Coping with danger, damage and death. *Cytokine Growth Factor Rev.* 22, 257–276.
- (2) Martinon, F., and Tschopp, J. (2005) NLRs join TLRs as innate sensors of pathogens. *Trends Immunol.* 26, 447–454.
- (3) Fritz, J. H., Ferrero, R. L., Philpott, D. J., and Girardin, S. E. (2006) Nod-like proteins in immunity, inflammation and disease. *Nat. Immunol.* 7, 1250–1257.
- (4) Martinon, F., Burns, K., and Tschopp, J. (2002) The inflammasome: A molecular platform triggering activation of inflammatory caspases and processing of proIL-1 $\beta$ . *Mol. Cell* 10, 417–426.

- (5) Petrilli, V., Dostert, C., Muruve, D. A., and Tschoopp, J. (2007) The inflammasome: A danger sensing complex triggering innate immunity. *Curr. Opin. Immunol.* 19, 615–622.
- (6) Ting, J. P., Lovering, R. C., Alnemri, E. S., Bertin, J., Boss, J. M., Davis, B. K., Flavell, R. A., Girardin, S. E., Godzik, A., Harton, J. A., Hoffman, H. M., Hugot, J. P., Inohara, N., Mackenzie, A., Maltais, L. J., Nunez, G., Ogura, Y., Otten, L. A., Philpott, D., Reed, J. C., Reith, W., Schreiber, S., Steimle, V., and Ward, P. A. (2008) The NLR gene family: A standard nomenclature. *Immunity* 28, 285–287.
- (7) Bao, Q., and Shi, Y. (2007) Apoptosome: A platform for the activation of initiator caspases. *Cell Death Differ.* 14, 56–65.
- (8) Martinon, F., Mayor, A., and Tschoopp, J. (2009) The inflammasomes: Guardians of the body. *Annu. Rev. Immunol.* 27, 229–265.
- (9) Hoffman, H. M., Mueller, J. L., Broide, D. H., Wanderer, A. A., and Kolodner, R. D. (2001) Mutation of a new gene encoding a putative pyrin-like protein causes familial cold autoinflammatory syndrome and Muckle-Wells syndrome. *Nat. Genet.* 29, 301–305.
- (10) Villani, A. C., Lemire, M., Fortin, G., Louis, E., Silverberg, M. S., Collette, C., Baba, N., Libioulle, C., Belaiche, J., Bitton, A., Gaudet, D., Cohen, A., Langelier, D., Fortin, P. R., Wither, J. E., Sarfati, M., Rutgeerts, P., Rioux, J. D., Vermeire, S., Hudson, T. J., and Franchimont, D. (2009) Common variants in the NLRP3 region contribute to Crohn's disease susceptibility. *Nat. Genet.* 41, 71–76.
- (11) Grenier, J. M., Wang, L., Manji, G. A., Huang, W. J., Al-Garawi, A., Kelly, R., Carlson, A., Merriam, S., Lora, J. M., Briskin, M., DiStefano, P. S., and Bertin, J. (2002) Functional screening of five PYPAF family members identifies PYPAF5 as a novel regulator of NF- $\kappa$ B and caspase-1. *FEBS Lett.* 530, 73–78.
- (12) Cui, J., Li, Y., Zhu, L., Liu, D., Songyang, Z., Wang, H. Y., and Wang, R. F. (2012) NLRP4 negatively regulates type I interferon signaling by targeting the kinase TBK1 for degradation via the ubiquitin ligase DTX4. *Nat. Immunol.* 13, 387–395.
- (13) Fiorentino, L., Stehlík, C., Oliveira, V., Ariza, M. E., Godzik, A., and Reed, J. C. (2002) A novel PAAD-containing protein that modulates NF- $\kappa$ B induction by cytokines tumor necrosis factor- $\alpha$  and interleukin-1 $\beta$ . *J. Biol. Chem.* 277, 35333–35340.
- (14) Zhang, P., Dixon, M., Zucchelli, M., Hambiliki, F., Levkov, L., Hovatta, O., and Kere, J. (2008) Expression analysis of the NLRP gene family suggests a role in human preimplantation development. *PLoS One* 3, e2755.
- (15) Jounai, N., Kobiyama, K., Shiina, M., Ogata, K., Ishii, K. J., and Takeshita, F. (2011) NLRP4 negatively regulates autophagic processes through an association with beclin1. *J. Immunol.* 186, 1646–1655.
- (16) Bae, J. Y., and Park, H. H. (2011) Crystal structure of NALP3 PYD domain and its implications in inflammasome assembly. *J. Biol. Chem.* 286, 39528–39536.
- (17) Hiller, S., Kohl, A., Fiorito, F., Herrmann, T., Wider, G., Tschoopp, J., Grutter, M. G., and Wuthrich, K. (2003) NMR structure of the apoptosis- and inflammation-related NALP1 pyrin domain. *Structure* 11, 1199–1205.
- (18) Liepinsh, E., Barbals, R., Dahl, E., Sharipo, A., Staub, E., and Otting, G. (2003) The death-domain fold of the ASC PYRIN domain, presenting a basis for PYRIN/PYRIN recognition. *J. Mol. Biol.* 332, 1155–1163.
- (19) Pinheiro, A. S., Eibl, C., Ekman-Vural, Z., Schwarzenbacher, R., and Peti, W. (2011) The NLRP12 Pyrin Domain: Structure, Dynamics, and Functional Insights. *J. Mol. Biol.* 413, 790–803.
- (20) Pinheiro, A. S., Proell, M., Eibl, C., Page, R., Schwarzenbacher, R., and Peti, W. (2010) Three-dimensional structure of the NLRP7 pyrin domain: Insight into pyrin-pyrin-mediated effector domain signaling in innate immunity. *J. Biol. Chem.* 285, 27402–27410.
- (21) Mueller, U., Darowski, N., Fuchs, M. R., Forster, R., Hellmig, M., Paithankar, K. S., Puhringer, S., Steffien, M., Zocher, G., and Weiss, M. S. (2012) Facilities for macromolecular crystallography at the Helmholtz-Zentrum Berlin. *J. Synchrotron Radiat.* 19, 442–449.
- (22) Kabsch, W. (2010) Xds. *Acta Crystallogr. D66*, 125–132.
- (23) Sheldrick, G. M. (2008) A short history of SHELX. *Acta Crystallogr. A64*, 112–122.
- (24) Sheldrick, G. M. (2010) Experimental phasing with SHELXC/D/E: Combining chain tracing with density modification. *Acta Crystallogr. D66*, 479–485.
- (25) Emsley, P., and Cowtan, K. (2004) Coot: Model-building tools for molecular graphics. *Acta Crystallogr. D60*, 2126–2132.
- (26) Adams, P. D., Afonine, P. V., Bunkoczi, G., Chen, V. B., Davis, I. W., Echols, N., Headd, J. J., Hung, L. W., Kapral, G. J., Grosjean-Kunstleve, R. W., McCoy, A. J., Moriarty, N. W., Oeffner, R., Read, R. J., Richardson, D. C., Richardson, J. S., Terwilliger, T. C., and Zwart, P. H. (2010) PHENIX: A comprehensive Python-based system for macromolecular structure solution. *Acta Crystallogr. D66*, 213–221.
- (27) Corpet, F. (1988) Multiple sequence alignment with hierarchical clustering. *Nucleic Acids Res.* 16, 10881–10890.
- (28) Holm, L., and Rosenstrom, P. (2010) Dali server: Conservation mapping in 3D. *Nucleic Acids Res.* 38, W545–W549.
- (29) Sippl, M. J. (2008) On distance and similarity in fold space. *Bioinformatics* 24, 872–873.
- (30) Sippl, M. J., and Wiederstein, M. (2008) A note on difficult structure alignment problems. *Bioinformatics* 24, 426–427.
- (31) Sippl, M. J., and Wiederstein, M. (2012) Detection of spatial correlations in protein structures and molecular complexes. *Structure* 20, 718–728.
- (32) Reynolds, C., Damerell, D., and Jones, S. (2009) ProtorP: A protein-protein interaction analysis server. *Bioinformatics* 25, 413–414.
- (33) *The PyMOL Molecular Graphics System*, version 1.2r3pre (2010) Schrödinger, LLC, New York.
- (34) Baker, N. A., Sept, D., Joseph, S., Holst, M. J., and McCammon, J. A. (2001) Electrostatics of nanosystems: Application to microtubules and the ribosome. *Proc. Natl. Acad. Sci. U.S.A.* 98, 10037–10041.
- (35) Richter, S., Wenzel, A., Stein, M., Gabdoulline, R. R., and Wade, R. C. (2008) webPIPSA: A web server for the comparison of protein interaction properties. *Nucleic Acids Res.* 36, W276–W280.
- (36) Gietz, R. D., and Woods, R. A. (2002) Transformation of yeast by lithium acetate/single-stranded carrier DNA/polyethylene glycol method. *Methods Enzymol.* 350, 87–96.
- (37) Wagner, R. N., Proell, M., Kufer, T. A., and Schwarzenbacher, R. (2009) Evaluation of Nod-like receptor (NLR) effector domain interactions. *PLoS One* 4, e4931.
- (38) Natarajan, A., Ghose, R., and Hill, J. M. (2006) Structure and dynamics of ASC2, a pyrin domain-only protein that regulates inflammatory signaling. *J. Biol. Chem.* 281, 31863–31875.
- (39) Jaroszewski, L., Rychlewski, L., Li, Z., Li, W., and Godzik, A. (2005) FFAS03: A server for profile–profile sequence alignments. *Nucleic Acids Res.* 33, W284–W288.
- (40) Stehlík, C., Krajewska, M., Welsh, K., Krajewski, S., Godzik, A., and Reed, J. C. (2003) The PAAD/PYRIN-only protein POP1/ASC2 is a modulator of ASC-mediated nuclear-factor- $\kappa$ B and pro-caspase-1 regulation. *Biochem. J.* 373, 101–113.
- (41) Weber, C. H., and Vincenz, C. (2001) The death domain superfamily: A tale of two interfaces? *Trends Biochem. Sci.* 26, 475–481.
- (42) Srimathi, T., Robbins, S. L., Dubas, R. L., Hasegawa, M., Inohara, N., and Park, Y. C. (2008) Monomer/dimer transition of the caspase-recruitment domain of human Nod1. *Biochemistry* 47, 1319–1325.
- (43) Manon, F., Favier, A., Nunez, G., Simorre, J. P., and Cusack, S. (2007) Solution structure of NOD1 CARD and mutational analysis of its interaction with the CARD of downstream kinase RIC. *J. Mol. Biol.* 365, 160–174.
- (44) Srimathi, T., Robbins, S. L., Dubas, R. L., Seo, J. H., and Park, Y. C. (2007) Purification, crystallization and preliminary crystallographic characterization of the caspase-recruitment domain of human Nod1. *Acta Crystallogr. F63*, 21–23.
- (45) Coussens, N. P., Mowers, J. C., McDonald, C., Nunez, G., and Ramaswamy, S. (2007) Crystal structure of the Nod1 caspase activation and recruitment domain. *Biochem. Biophys. Res. Commun.* 353, 1–5.

- (46) Tattoli, I., Travassos, L. H., Carneiro, L. A., Magalhaes, J. G., and Girardin, S. E. (2007) The Nodosome: Nod1 and Nod2 control bacterial infections and inflammation. *Semin. Immunopathol.* 29, 289–301.
- (47) Kersse, K., Versputen, J., Vanden Berghe, T., and Vandenebeele, P. (2011) The death-fold superfamily of homotypic interaction motifs. *Trends Biochem. Sci.* 36, 541–552.
- (48) Innis, C. A., Shi, J., and Blundell, T. L. (2000) Evolutionary trace analysis of TGF- $\beta$  and related growth factors: Implications for site-directed mutagenesis. *Protein Eng.* 13, 839–847.
- (49) Liu, T., Rojas, A., Ye, Y., and Godzik, A. (2003) Homology modeling provides insights into the binding mode of the PAAD/DAPIN/pyrin domain, a fourth member of the CARD/DD/DED domain family. *Protein Sci.* 12, 1872–1881.
- (50) Srimathi, T., Robbins, S. L., Dubas, R. L., Chang, H., Cheng, H., Roder, H., and Park, Y. C. (2008) Mapping of POP1-binding site on pyrin domain of ASC. *J. Biol. Chem.* 283, 15390–15398.
- (51) Park, H. H., Logette, E., Raunser, S., Cuenin, S., Walz, T., Tschoopp, J., and Wu, H. (2007) Death domain assembly mechanism revealed by crystal structure of the oligomeric PIDDosome core complex. *Cell* 128, 533–546.
- (52) Scott, F. L., Stec, B., Pop, C., Dobaczewska, M. K., Lee, J. J., Monosov, E., Robinson, H., Salvesen, G. S., Schwarzenbacher, R., and Riedl, S. J. (2009) The Fas-FADD death domain complex structure unravels signalling by receptor clustering. *Nature* 457, 1019–1022.
- (53) Zhou, P., Chou, J., Olea, R. S., Yuan, J., and Wagner, G. (1999) Solution structure of Apaf-1 CARD and its interaction with caspase-9 CARD: A structural basis for specific adaptor/caspase interaction. *Proc. Natl. Acad. Sci. U.S.A.* 96, 11265–11270.
- (54) Manji, G. A., Wang, L., Geddes, B. J., Brown, M., Merriam, S., Al-Garawi, A., Mak, S., Lora, J. M., Briskin, M., Jurman, M., Cao, J., DiStefano, P. S., and Bertin, J. (2002) PYPAF1, a PYRIN-containing Apaf1-like protein that assembles with ASC and regulates activation of NF- $\kappa$ B. *J. Biol. Chem.* 277, 11570–11575.
- (55) Martinon, F., Hofmann, K., and Tschoopp, J. (2001) The pyrin domain: A possible member of the death domain-fold family implicated in apoptosis and inflammation. *Curr. Biol.* 11, R118–R120.
- (56) Damiano, J. S., Oliveira, V., Welsh, K., and Reed, J. C. (2004) Heterotypic interactions among NACHT domains: Implications for regulation of innate immune responses. *Biochem. J.* 381, 213–219.
- (57) Zhou, P., and Wagner, G. (2010) Overcoming the solubility limit with solubility-enhancement tags: Successful applications in biomolecular NMR studies. *J. Biomol. NMR* 46, 23–31.
- (58) Tian, X., Pascal, G., and Monget, P. (2009) Evolution and functional divergence of NLRP genes in mammalian reproductive systems. *BMC Evol. Biol.* 9, 202.
- (59) Qin, H., Srinivasula, S. M., Wu, G., Fernandes-Alnemri, T., Alnemri, E. S., and Shi, Y. (1999) Structural basis of procaspase-9 recruitment by the apoptotic protease-activating factor 1. *Nature* 399, 549–557.
- (60) de Alba, E. (2009) Structure and interdomain dynamics of apoptosis-associated speck-like protein containing a CARD (ASC). *J. Biol. Chem.* 284, 32932–32941.
- (61) Esposito, D., Sankar, A., Morgner, N., Robinson, C. V., Rittinger, K., and Driscoll, P. C. (2010) Solution NMR investigation of the CD95/FADD homotypic death domain complex suggests lack of engagement of the CD95 C terminus. *Structure* 18, 1378–1390.
- (62) Park, H. H. (2011) Structural analyses of death domains and their interactions. *Apoptosis* 16, 209–220.
- (63) Weiss, M. S. (2001) Global indicators of X-ray data quality. *J. Appl. Crystallogr.* 34, 130–135.
- (64) Collaborative Computational Project, Number 4 (1994) The CCP4 suite: Programs for protein crystallography. *Acta Crystallogr. D50*, 760–763.
- (65) Tickle, I. J., Laskowski, R. A., and Moss, D. S. (1998) Error estimates of protein structure coordinates and deviations from standard geometry by full-matrix refinement of  $\gamma$ B- and  $\beta$ B2-crystallin. *Acta Crystallogr. D54*, 243–252.